Korean J. Chem. Eng., 39(12), 3267-3276 (2022)
DOI: 10.1007/s11814-022-1208-y

pISSN: 0256-1115
eISSN: 1975-7220

Enhanced photocatalytic activity over ZnO supported on calcium sulfate whisker derived from desulfurization gypsum

Shijing Lin*, Yu Tian, Wei Zhang*,†, Tiantian Zhao*, Mingxin Zhao*, and Hong Wang*,†**

*Beijing Key Laboratory of Fuels Cleaning and Advanced Catalytic Emission Reduction Technology, College of New Materials and Chemical Engineering, Beijing Institute of Petrochemical Technology, Beijing 102617, P. R. China
**Beijing Origin Water Membrane Technology Company, Beijing 102617, P. R. China
(*Received 12 February 2022 • Revised 6 June 2022 • Accepted 15 June 2022*)

Abstract−Calcium sulfate whisker (CSW) was prepared from flue gas desulfurization (FGD) gypsum by recrystallization method, and then was employed in preparing ZnO/CSW photocatalysts by impregnation method. CSW and ZnO/CSW were characterized by scanning electron microscopy (SEM), transmission electron microscopy (TEM), X-ray diffraction (XRD), X-ray photoelectron spectroscopy (XPS), Fourier transform infrared spectroscopy (FT-IR), UV-Vis diffuse reflectance spectroscopy (UV-Vis DRS) and photoluminescence spectrum (PL). The photocatalytic activity of various ZnO/CSW photocatalysts was evaluated by photocatalytic degradation of methylene blue (MB) under simulated sunlight irradiation. The results showed that various ZnO/CSW photocatalysts exhibited much higher photocatalytic activity than pure ZnO and CSW. Among various ZnO/CSW photocatalysts, the photocatlytic activity of ZnO/CSW increased as increasing the ZnO loading amount from 1.2% to 8.7%, but decreased when the ZnO loading amount was beyond 8.7% due to the increasing crystalline size of ZnO and recombination of photogenerated hole/electron pairs. Besides ZnO loading amount, MB initial concentration and the dosage of photocatalyst also had significant influence on MB degradation rate, and MB degradation rate over ZnO/CSW reached 95.4% under optimum conditions. Kinetics study revealed that the photocatalytic degradation of MB over ZnO/CSW can be described by the pseudo-first-order kinetic model, and the apparent rate constant k versus ZnO loading amount L, MB initial concentration C_0 and the dosage of photocatalyst D can be described as: $k=0.5237L^{0.5193}C_0^{-0.3074}D^{0.4589}$.

Keywords: Desulfurization Gypsum, Calcium Sulfate Whisker, ZnO, Photocatalysis, Methylene Blue

INTRODUCTION

Flue gas desulfurization (FGD) gypsum is the second largest solid residual of thermal power plants produced from the wet desulfurization process [1]. Due to its low quality and utilization potential, tremendous FGD has been discarded, which not only pollutes soil and water, but also endangers the human respiratory system when floating in the atmosphere [2]. Therefore, it is highly desired to recycle and utilize FGD. Converting FGD gypsum to calcium sulfate whisker (CSW) is a potential way to realize FGD gypsum utilization because CSW has high mechanical strength and slenderness ratio, is nontoxic and resistant to high temperature, acid and alkali [2-5]. Currently, CSW is widely used in papermaking, rubber, plastics [6-8], friction materials [9] and wastewater treatment. However, the market demand for CSW is relatively low in comparison with the tremendous production of FGD gypsum. Hence, it is highly demanded to explore the new application of CSW derived from FGD gypsum.

Recently, water pollution caused by dye discharges from various industries (such as papermaking, textile dyeing, cosmetics, paint and food) has attracted extensive attention, due to the toxicity and carcinogenicity, and xenobiotic [10,11]. Among those, thiazide dyes are the most common colorants, and methylene blue (MB) is a typical representative of thiazide dyes [12]. MB is a popular dyeing material for wood, silk and cotton, and also in medical fields to identify some diseases [13]. The exposure of MB can lead to vomiting, eye infection, diarrhea, nausea and other diseases. Hence, it is imperative to remove MB from the wastewater [14]. The traditional wastewater treatment technologies include adsorption, coagulation and sedimentation, which usually require a long operation time, produce secondary sludge, and have high treatment cost [15].

In the past decades, photocatalysis technology has drawn extensive attention in the field of energy production and environmental remediation, due to the advantages of strong oxidizability, high energy efficiency, mild reaction condition, and environmental friendliness [16,17]. Many studies have shown that photocatalysis is effective in degrading colorants in water [12]. Due to high photocatalysis efficiency, low cost, high stability and nontoxicity, ZnO has been one of the most promising photocatalysts [18]. Nevertheless, pure ZnO photocatalyst usually presents poor photocatalytic activity due to its large crystalline size. Modification by doping or supporting is an effective method to improve its photocatalytic activity [18-21].

In this work, to improve the photocatalytic activity of ZnO, CSW was employed as the support to prepare ZnO/CSW photocatalyst. CSW was prepared using FGD gypsum from a thermal power plant, and ZnO/CSW was prepared by impregnation method. Various ZnO/CSW photocatalysts were characterized, and also taken for photocatalytic degradation of MB under simulated sunlight irradi-

†To whom correspondence should be addressed.
E-mail: wzhang@bipt.edu.cn, wanghong@bipt.edu.cn

ation to test their photocatalytic activity. Influences of ZnO loading amount, the initial MB concentrations, and the photocatalyst dosage on the degradation of MB were investigated. Moreover, the photocatalytic degradation kinetics of methylene blue by ZnO/CSW was analyzed and discussed.

EXPERIMENTAL

1. Materials

FGD gypsum used in the experiment was obtained from Guohua Dingzhou Power Plant, China. Sulfuric acid and zinc nitrate (analytical pure) were purchased from Sinopharm Chemical Reagent Co., Ltd., China, and used without further purification.

2. Preparation of CSW and ZnO/CSW

2-1. Preparation of CSW

Calcium sulfate whisker was prepared using FGD gypsum from a thermal power plant. The preparation procedure was as follows: First, 100 g of FGD gypsum was pretreated with 200 mL of 3.55 mmol/L dilute sulfuric acid solution. The resulting mixture was stirred vigorously at room temperature for 30 min until no bubbles were generated. After filtration, the filter cake was washed with deionized water for several times, and then dried in the oven at 80 °C for 6 h. The pretreated FGD gypsum was then crushed and sieved to less than 100 meshes. Second, 10 g of the pretreated desulfurized gypsum was added to 300 mL of 2 mol/L sulfuric acid solution, and then acidized at 80 °C for 1 h under stirring, followed by hot filtration to remove the impurity. Afterwards, the obtained filtrate was cooled to 30 °C by recrystallization method. After aging for 3 h, the resulting CSW was filtrated, washed with deionized water for several times, and dried in an oven at 90 °C for 2 h.

2-2. Preparation of ZnO/CSW and ZnO

ZnO/CSW was prepared by impregnation method with FGD gypsum-derived CSW as the support. A predetermined amount of zinc nitrate was dissolved in 40 mL of deionized water, and then 4 g of calcium sulfate whisker was added in. The resulting mixture was stirred at room temperature for 1 h and then evaporated by a rotary evaporator under vacuum at 60 °C to remove water. Afterwards, the catalyst precursor was dried at 110 °C and then calcined at 400 °C for 2 h. The obtained ZnO/CSW with different ZnO loading amounts was labeled as ZnO(x)/CSW, where x refers to the loading amount of ZnO. Pure ZnO was prepared by direct calcination of $Zn(NO_3)_2$ at 400 °C for 2 h.

3. Characterization

The SEM and TEM images of CSW and ZnO/CSW were obtained on a S-4800 high-resolution scanning electron microscope (Hitachi High Tech Co., Japan) and Tecnai G2 field emission transmission electron microscope (FEI Co., USA), respectively. Powder X-ray diffraction patterns of the samples were recorded using a D/max 2600/PC powder diffractometer (Rigaku, Japan) with Cu Kα anode at a scanning rate of 1°/min in the 2θ range of 10-70° with the voltage of 40 kV and the current of 100 mA (λ=0.15418 nm). UV-Vis diffuse reflection spectra were recorded on a UV-2300 spectrometer (Hitachi High Tech Co., Ltd., Japan) from 200 nm to 800 nm using $BaSO_4$ as the reference. Photoluminescence spectra (PL) of the samples were obtained on an FS-5 spectrophotometer (Edinburgh, England) at a scanning rate of 1,200 nm·min^{-1} with an excitation wavelength of 325 nm. The FT-IR spectra of samples were recorded on a TENSOR 27 infrared spectrometer (Bruker, Germany) at a resolution of 4 cm^{-1}. X-ray photoelectron spectroscopy (XPS) characterization was performed on an ESCALAB 250 photoelectron spectroscope (Thermo Fisher Scientific, USA) equipped with Mg Kα anode. All the spectra were calibrated against the major C 1s peak at a binding energy of 284.6 eV.

4. Photocatalytic Degradation of Methylene Blue

Photocatalytic degradation of methylene blue was conducted in a photochemical reactor (CEL-HXUV300E, Beijing Zhongjiaojinyuan Co., Ltd., China) to evaluate the photocatalytic activity of various ZnO(x)/CSW. As reported in our previous paper [22], the reaction system consists of a 300 W xenon lamp to simulate sunlight, a circulator bath to control the temperature, a glass reactor and a magnetic stirrer. In a typical run, 100 mL of 10 mg/L methylene blue solution (pH=7.0) and 0.1 g of ZnO/CSW were added in the reactor. The mixture was stirred vigorously and kept at 25 °C by a circulator bath throughout the experiment. After the simulated sunlight irradiation was introduced, the mixture was sampled periodically at intervals of 30 min and filtered. The samples were then analyzed using a UV-visible spectrophotometer at the absorption wavelength of 664 nm. The concentration of methylene blue was determined according to the standard curve (Fig. S1), and the degradation rate of methylene blue was calculated by Eq. (1):

$$x = \frac{C_0 - C_t}{C_0} \times 100\% \quad (1)$$

where x is the degradation rate of methylene blue at irradiation time t, %; C_0 is the initial MB concentration and C_t is the MB concentration at irradiation time t, mg/L.

RESULTS AND DISCUSSION

1. Characterization of CSW and ZnO(x)/CSW

Fig. 1 presents the SEM images of CSW and ZnO(8.7)/CSW. It is visible in Fig. 1(a) that the surface of CSW is relatively smooth. In contrast, the surface of ZnO(8.7)/CSW is very rough, suggesting small ZnO particles were deposited on the surface of CSW. According to EDS images in Fig. S2, CSW mainly contains O, S and Ca, indicating no impurity was present in CSW; ZnO(8.7)/CSW contains Zn element besides O, S and Ca, confirming the loading of ZnO on CSW.

Fig. 2 shows the TEM images of ZnO(8.7)/CSW and ZnO (11.2)/CSW. It can be seen from Fig. 2(a), (b) that the distribution of ZnO in ZnO(8.7)/CSW is relatively uniform, while ZnO in ZnO(11.2)/CSW is obviously accumulated, indicating the ZnO loading amount higher than 8.7% will lead to the agglomeration of ZnO.

Fig. 3 shows the XPS spectra of CSW and ZnO(x)/CSW (x= 6.2, 8.7, 11.2). It can be seen from XPS survey of ZnO(x)/CSW in Fig. 3(a) that CSW is composed of S, Ca and O elements, while ZnO(x)/CSW consists of Zn, S, Ca and O elements, which is in good agreement with the EDS results in Fig. S2. Fig. 3(b) exhibits the high-resolution Zn 2p spectra of ZnO(x)/CSW. It is seen that two different binding energy sites are located at 1,021.5 eV and 1,044.6 eV, which can be assigned to Zn $2P_{3/2}$ and Zn $2p_{1/2}$ in Zn^{2+} oxidation state [23-25], respectively, indicating that the Zn species on

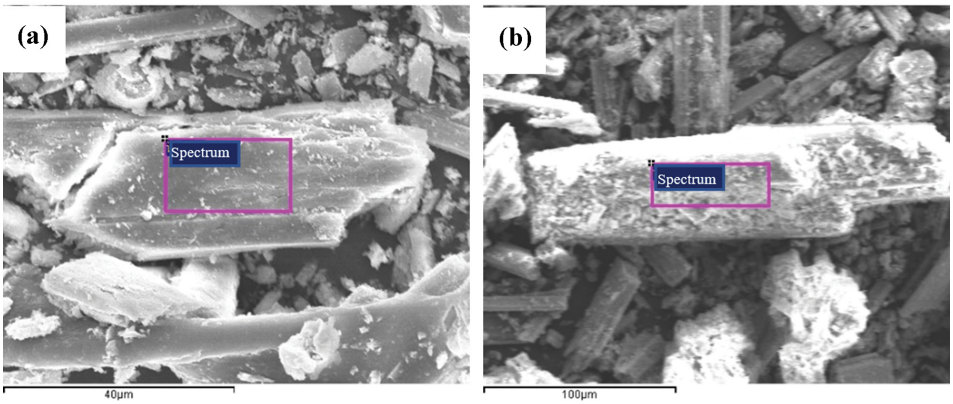

Fig. 1. SEM images of CSW (a) and ZnO(8.7)/CSW (b).

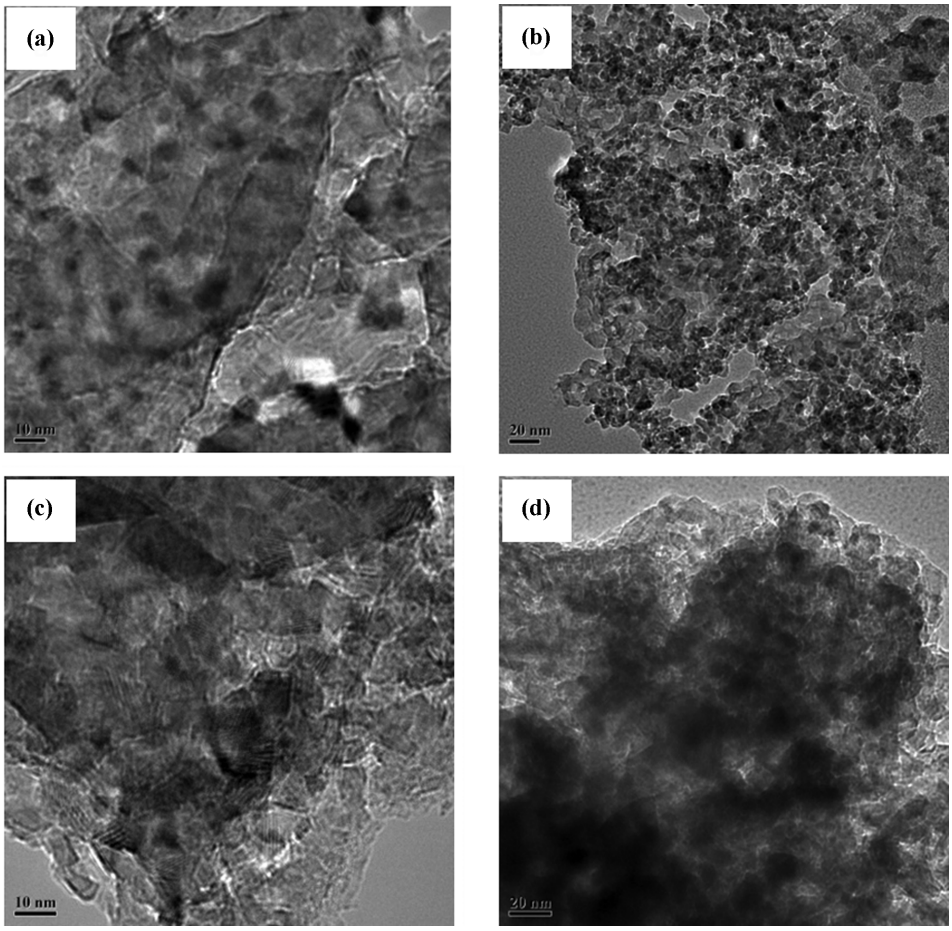

Fig. 2. TEM of (a), (b) ZnO(8.7)/CSW and (c), (d) ZnO(11.2)/CSW.

the catalysts was ZnO. According to Fig. 3(c), the characteristic peak of O 1s appears at 532.5 eV, attributed to Zn-O, S-O or adsorbed -OH [26]. As shown in Fig. 3(d), the characteristic diffraction peak of S 2p is centered at 169.43 eV. Fig. 3(e) shows that the characteristic diffraction peak of Ca 2p is located at 348.13 eV.

Fig. 4 illustrates the XRD patterns of CSW and ZnO(x)/CSW. It can be observed from Fig. 4(a) that CSW shows clear characteristic peaks at 2θ=25.5°, 31.4°, 38.7°, 40.9°, 48.8° and 55.9°, which are corresponding to (020), (210), (220), (212), (230) and (232) crystal planes of $CaSO_4$ (PDF No. 74-2421), respectively. In comparison to CSW, the characteristic peak intensity of $CaSO_4$ for various ZnO(x)/CSW had no obvious decrease, indicating that the crystal structure of CSW in ZnO(x)/CSW remained unchanged. From the enlarged view in Fig. 4(b), it is visible that the characteristic diffraction peak at 2θ=34.6° corresponding to the (002) plane reflection of ZnO (PDF No. 79-0205) [27] appeared when ZnO loading

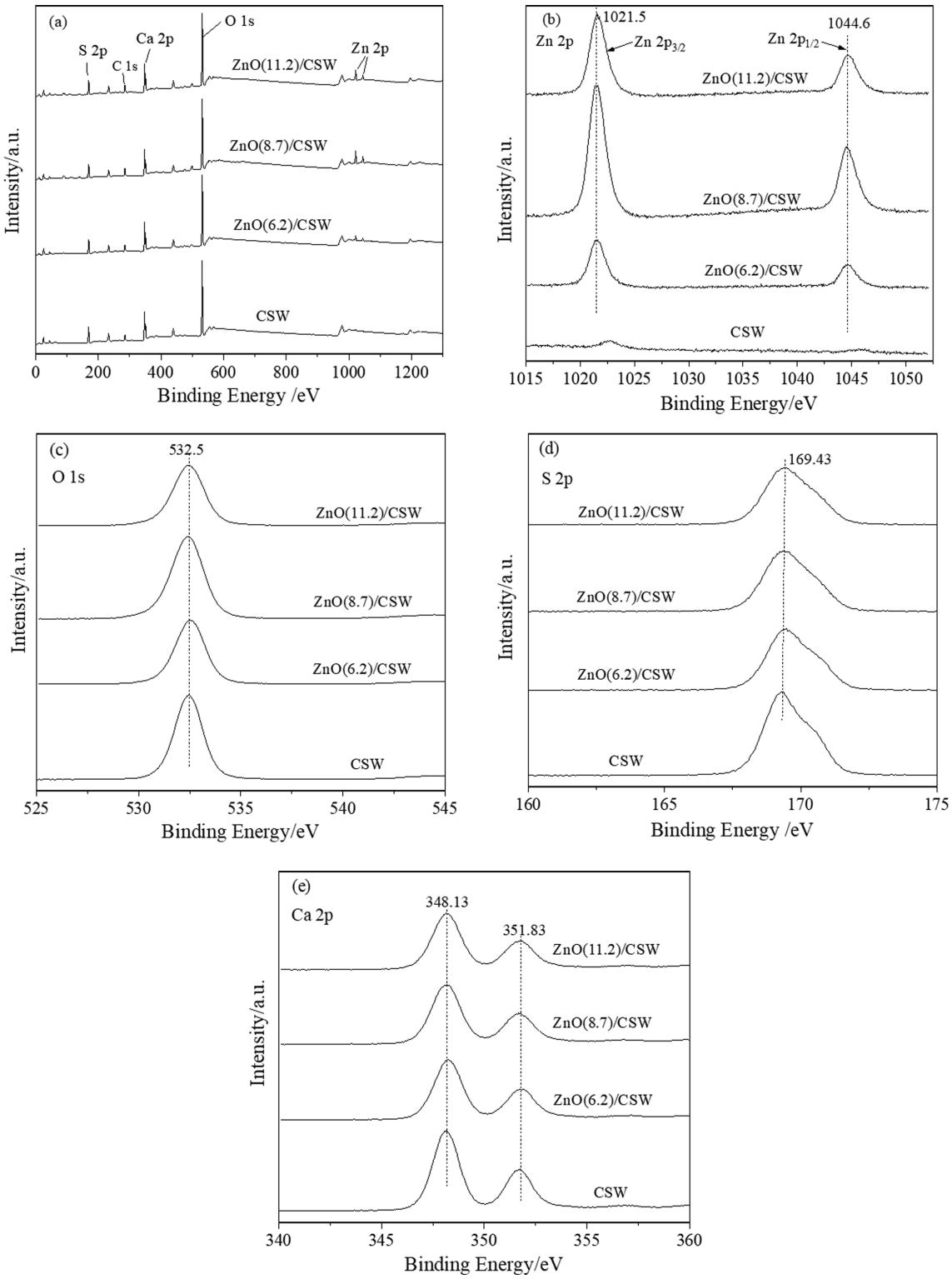

Fig. 3. XPS spectra of ZnO(x)/CSW ((a) survey; (b) Zn 2p; (c) O 1s; (d) S 2p; (e) Ca 2p).

amount in ZnO(x)/CSW was higher than 2.5% and increased with increasing ZnO loading amount. Moreover, the overlapped characteristic diffraction peaks of ZnO at 31.9° and 36.4° with the characteristic diffraction peaks of CSW also clearly increased with the increase of ZnO loading amount, and there was an obvious increase of the diffraction peaks when ZnO loading amount was beyond 10%, indicating the obvious increase of ZnO crystalline size for ZnO loading amount higher than 10%.

Fig. 5 shows the FT-IR spectra of CSW and ZnO(x)/CSW. Two strong absorption peaks at around 3,611 cm^{-1} and 3,396 cm^{-1} on

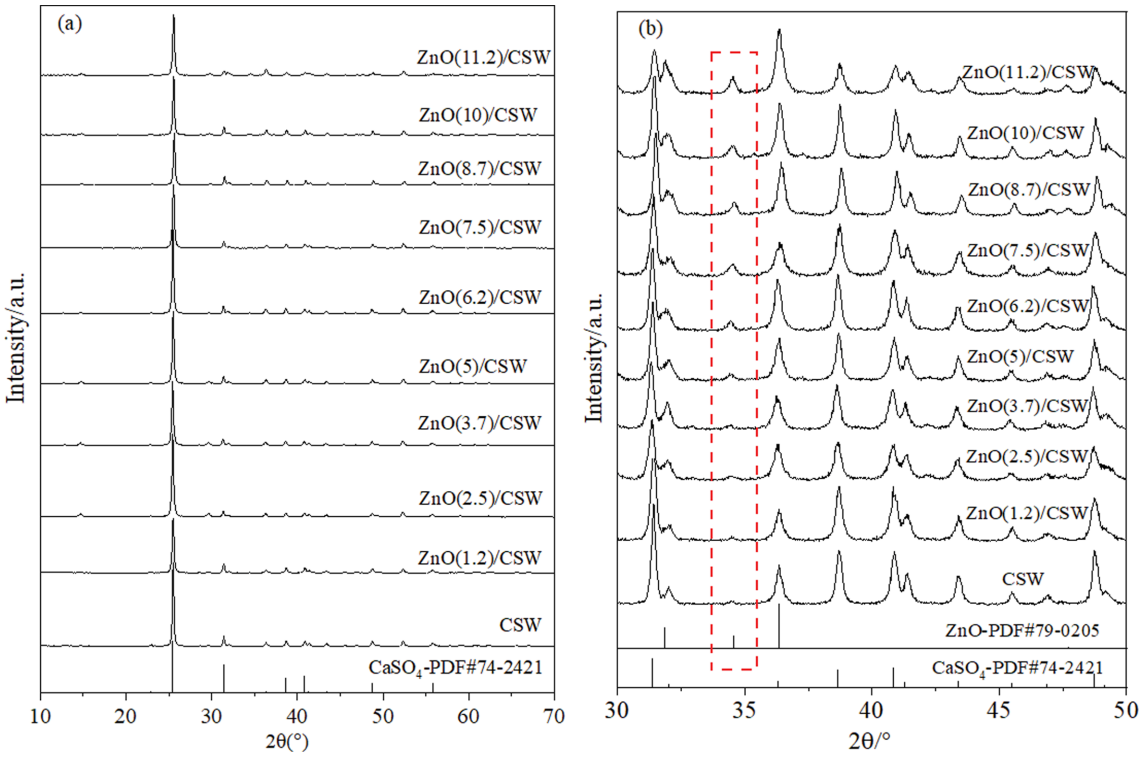

Fig. 4. XRD patterns of CSW and various ZnO(x)/CSW (a) full curves; (b) partial enlarged view).

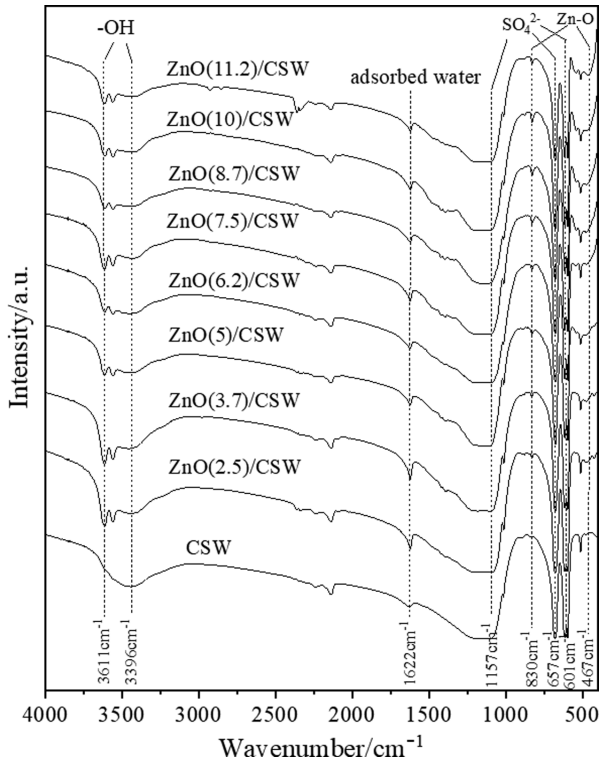

Fig. 5. FT-IR spectra of CSW and ZnO(x)/CSW.

ZnO(x)/CSW are corresponding to the stretching vibrations of -OH groups on ZnO and CSW [24-26], respectively, which are beneficial to the adsorption of organic dyes [16,28]. All the samples show the bending vibration absorption of the adsorbed water at 1,622 cm^{-1} [29], and tensile vibration and bending vibration peaks of SO_4^{2-} at 1,157 cm^{-1}, 657 cm^{-1} and 601 cm^{-1} [30,31]. ZnO(x)/CSW exhibits two absorption peaks at 830 cm^{-1} and 467 cm^{-1}, which are attributed to the stretching vibration of Zn-O bond [32].

Fig. 6 shows UV-Vis diffuse reflectance spectra of CSW and ZnO(x)/CSW. It can be seen from Fig. 6(a) that pure CSW has no obvious UV-Vis absorption. When CSW was loaded with 1.2% ZnO, an obvious absorption in the UV region was observed, and UV absorption of various ZnO(x)/CSW increased with the increase of the ZnO loading amount. Moreover, the absorption edge gradually increased with increasing the ZnO loading amount.

The band gap energy (E_g) of ZnO(x)/CSW photocatalysts can been further obtained by Tauc's plot [32] with Eq. (2).

$$(\alpha h\nu)^{1/n} = A(h\nu - E_g) \quad (2)$$

where α is the absorption coefficient, hv is the photon energy, E_g is the band gap and A is a constant. Since ZnO is a direct band gap semiconductor [33], n is 1/2. The fitting curves are illustrated in Fig. 6(b) and the obtained band gap energies of ZnO(x)/CSW are listed in Table S2. It can be seen from Table S2 that the band gaps of various ZnO(x)/CSW are in the range of 3.272-3.299 eV, which are slightly lower than that of pure ZnO (E_g=3.37 eV) reported in the literature [34], indicating the wider UV-Vis adsorption range of ZnO(x)/CSW than pure ZnO.

It is well known that PL can be used to evaluate the recombination rate of photogenerated hole/electron pairs, and lower PL intensity means the less recombination of photogenerated hole/electron

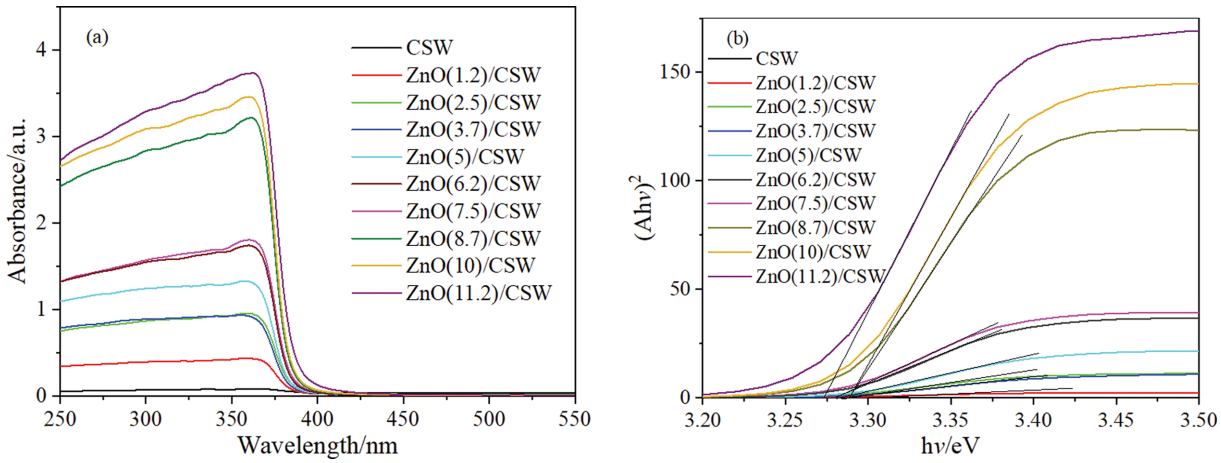

Fig. 6. (a) UV-Vis DRS spectra of ZnO(x)/CSW; (b) Tauc plots of ZnO(x)/CSW.

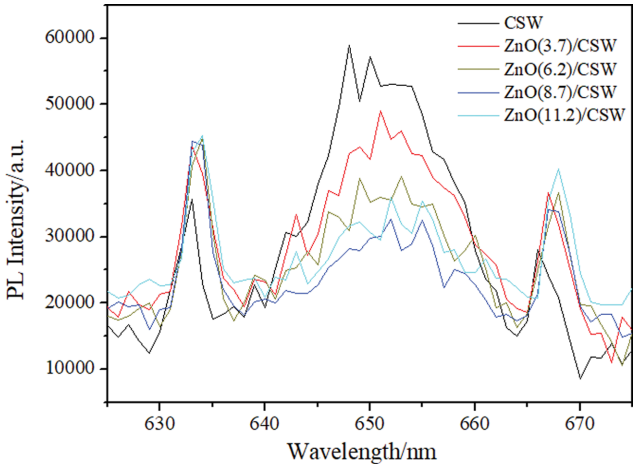

Fig. 7. Fluorescence spectra of ZnO(x)/CSW.

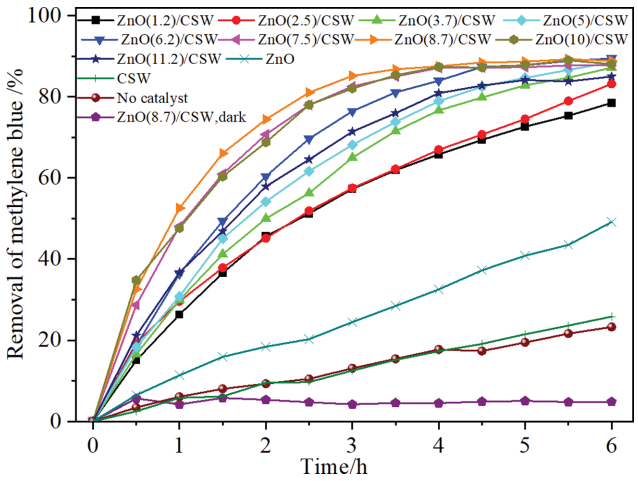

Fig. 8. Photocatalytic degradation of MB over ZnO(x)/CSW (MB initial concentration, 10 mg/L; dosage of the photocatalyst, 1%).

pairs. Fig. 7 gives the PL spectra of ZnO(x)/CSW (x=0, 3.7, 6.2, 8.7, 11.2), which were obtained at room temperature with an excitation wavelength of 325 nm. It is evident in Fig. 7 that various ZnO(x)/CSW show a main PL peak in the wavelength range of 640-660 nm, and the PL intensity of ZnO(x)/CSW in the wavelength range of 640-660 nm decreased with increasing ZnO loading amount to 8.7%, but slightly increased when the loading amount was beyond 8.7%, probably due to the increase of ZnO crystallize size. The above results indicate that ZnO(8.7)/CSW had the highest separation efficiency of photogenerated hole/electron pairs.

2. Photocatalytic Degradation of MB

2-1. Influence of ZnO Loading Amount

Fig. 8 presents the photocatalytic degradation of MB over CSW and ZnO(x)/CSW with/without simulated sunlight irradiation. It is observed from Fig. 8 that in the presence of ZnO(8.7)/CSW, but without simulated sunlight irradiation, MB removal is within 5% after adsorption for 6 h. However, under simulated sunlight irradiation, but without the presence of a catalyst, MB removal reached 23.3% at the irradiation time of 6 h, which could be ascribed to the photolysis of MB. When CSW was introduced, MB removal was only 25.85% after 6 h of irradiation, which was only 2.58% higher than that in the absence of a catalyst, indicating that CSW had almost no photocatalytic activity. Many studies have shown that sulfate radical ($SO_4^{\cdot-}$) has strong decomposing ability for organic substances, and sulfate radical-based advanced oxidation technologies have been applied to removing pollutants from wastewater generated in various environments [35]. However, in this work, CSW had almost no photocatalytic activity, indicating $SO_4^{\cdot-}$ was not involved in the degradation of MB. When pure ZnO was employed as the photocatalyst, the degradation rate of MB was only 49.15% after 6 h of light irradiation, much lower than ZnO(x)/CSW. In a sharp contrast, when CSW was loaded with 1.2% ZnO, the MB degradation rate sharply increased to 78.5% probably due to high dispersion and smaller crystalline size of ZnO on CSW, and the degradation rate of MB over ZnO(x)/CSW continued to increase with increasing ZnO loading amount further to 8.7% due to the increase of the active sites and faster separation of photogenerated hole/electron pair. The degradation rate of MB over ZnO(8.7)/CSW reached 88.9% after 6 h of light irradiation. However, the photocatalytic activity of ZnO(x)/CSW gradually decreased when ZnO

loading amount was beyond 8.7%. It was known from the previous TEM (Fig. 2) and XRD characterization (Fig. 4) results that the characteristic diffraction peaks of ZnO increased with the increase of ZnO loading amount, and PL results (Fig. 7) revealed that the main PL peak of ZnO(x)/CSW decreased with increasing ZnO loading amount to 8.7%, but slightly increased when the loading amount was beyond 8.7%. Hence, the decrease of the photocatalytic activity of ZnO(x)/CSW when ZnO loading amount was beyond 8.7% could be ascribed to the increase of ZnO loading amount and more recombination of photogenerated hole/electron pairs [36]. The above results demonstrate that CSW-supported ZnO exhibited superior photocatalytic activity and is a promising photocatalyst for the degradation of organic dyes.

2-2. Influence of MB Initial Concentration

Fig. 9 shows the photocatalytic degradation of MB with different initial concentrations over ZnO(8.7)/CSW. It is clear that the degradation rate of MB decreased with increasing the initial concentration of MB, implying ZnO(x)/CSW had lower photocatalysis efficiency for the degradation of MB with higher initial concentration. However, the degradation rate of MB might have been enhanced by increasing the photocatalyst dosage, which will be addressed in the following section.

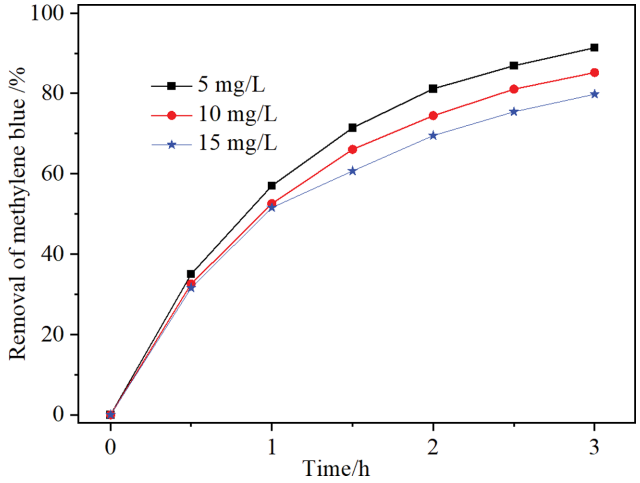

Fig. 9. Photocatalytic degradation of MB with different initial concentrations over ZnO(8.7)/CSW (dosage of photocatalyst, 1%).

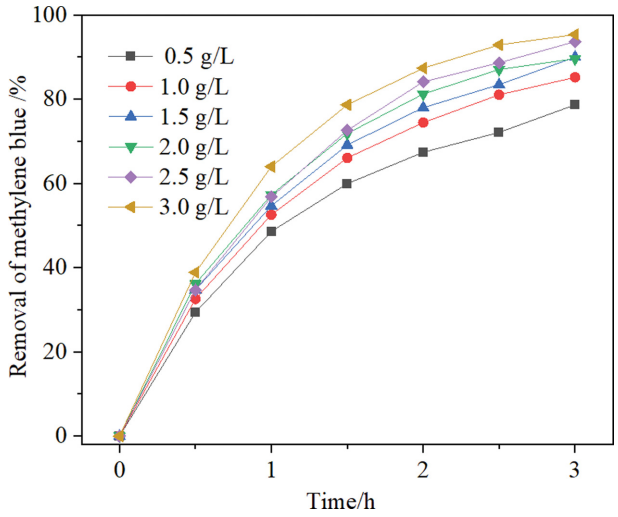

Fig. 10. Influence of the dosage of ZnO(8.7)/CSW on the photocatalytic degradation of MB (MB initial concentration, 10 mg/L).

2-3. Influence of Photocatalyst Dosage

Fig. 10 presents the photocatalytic degradation of MB by different dosage of ZnO(8.7)/CSW. It is observed that the degradation rate of MB increased from 78.7% to 95.4% at the irradiation time of 3 h with increasing the dosage of ZnO(8.7)/CSW from 0.5 g/L to 3 g/L, suggesting the positive effect of increasing the dosage of photocatalyst.

3. Photocatalytic Degradation Kinetics of MB over ZnO(x)/CSW

To quantitatively examine the influence of ZnO loading amount, the initial concentration of methylene blue and the dosage of ZnO(x)/CSW on the degradation of MB, the photocatalytic degradation kinetics of MB over ZnO(x)/CSW were investigated using the Langmuir Hinshelwood (L-H) model, which has been extensively employed to describe the photocatalytic degradation kinetics of organic pollutants in aqueous phase [37,38], as given below:

$$r = -\frac{dC_t}{dt} = \frac{k_r K C_t}{(1+KC_0)} \quad (3)$$

where r or $(-dC_t/dt)$ represents the degradation rate of MB, C_0 is the initial concentration of MB, C_t is the MB concentration at reaction time t, k_r is the reaction rate constant, and K is the adsorption equilibrium constant. Because adsorption affinity of ZnO(x)/CSW for MB is relatively weak and the concentration of MB is very low in this work, KC_0 can be ignored, and $\frac{k_r K C_t}{(1+KC_0)} \approx k_r K C_t$,

Furthermore, Eq. (3) can be simplified as a pseudo-first-order kinetic equation, as described in Eq. (4).

$$\ln\frac{C_0}{C_t} = kt \quad (4)$$

where k (h^{-1}) is the apparent reaction rate constant.

When plotting $\ln(C_0/C)$ as a function of the irradiation time (t), k can be obtained from the slope of the fitted straight line.

Based on the data in Figs. 8-10, the relationship between $\ln(C_0/C)$ and the irradiation time (t) was plotted and fitted by straight lines in Fig. S3-S5, and the correlation coefficients and obtained k were listed in Tables 1-3, respectively. It can be seen that in each plot, $\ln(C_0/C_t)$ is basically linear with irradiation time t, and all the correlation coefficients are beyond 0.99, indicating the degradation of methylene blue by ZnO(x)/CSW approximately obeyed L-H pseudo-first-order kinetics.

Normally, in a heterogeneous catalytic reaction system, there are many factors affecting the apparent reaction rate constant k [36]. From the discussion above, it is known that the ZnO loading amount, MB initial concentration and dosage of ZnO(x)/CSW have significant influences on the photocatalytic degradation of MB. It is assumed that the relationship between k and the three influencing factors can be described as Eq. (5):

$$k = f(L, C_0, D) = \mu L^{\alpha} C_0^{\beta} D^{\gamma} \quad (5)$$

Table 1. The fitted equations and parameters of MB photocatalytic degradation over ZnO(x)/CSW from Fig. S3 using pseudo-first kinetic model

ZnO loading/%	Fitted linear equation	k/h^{-1}	R^2
1.2	y=0.2458x+0.0390	0.2458	0.9966
2.5	y=0.2556x+0.0910	0.2556	0.9998
3.7	y=0.3384x+0.0143	0.3384	0.9968
5.0	y=0.4686x+0.0015	0.4686	0.9963
6.2	y=0.4955x−0.0489	0.4955	0.9994
7.5	y=0.5660x+0.0801	0.5660	0.9983
8.7	y=0.6070x+0.1314	0.6070	0.9965
10.0	y=0.5311x+0.1369	0.5311	0.9959
11.2	y=0.4029x+0.0422	0.4029	0.9988

Table 2. The fitted equations and parameters of photocatalytic degradation of MB with different initial concentrations from Fig. S4 using pseudo-first kinetic model

MB initial concentration/$mg\cdot L^{-1}$	Fitted linear equation	k/h^{-1}	R^2
5	y=0.4992x+0.0760	0.4992	0.9962
10	y=0.3932x+0.0531	0.3932	0.9990
15	y=0.3579x+0.0796	0.3579	0.9989

Table 3. The fitted equations and parameters of photocatalytic degradation of MB under different dosages of ZnO(8.7)/CSW from Fig. S5 using pseudo-first kinetic model

Photocatalyst dosage ($g\cdot L^{-1}$)	Fitted linear equation	k/h^{-1}	R^2
0.5	y=0.3155x+0.0556	0.3155	0.9986
1.0	y=0.3932x+0.0531	0.3932	0.9990
1.5	y=0.5531x+0.0667	0.5531	0.9984
2.0	y=0.5627x+0.1160	0.5627	0.9924
2.5	y=0.6577x+0.0221	0.6577	0.9980
3.0	y=0.6967x+0.1060	0.6967	0.9939

where μ is a constant, L represents the ZnO loading amount in ZnO(x)/CSW, C_0 is the initial concentration of MB (mg/L) and D is the photocatalyst dosage (g/L).

Through taking the log of both sides, Eq. (5) can be transformed to Eq. (6).

$$\ln k = \ln\mu + \alpha \ln L + \beta \ln C_0 + \gamma \ln D \quad (6)$$

If lnk versus lnL, $\ln C_0$ and lnD are plotted and linearly fitted, α, β and γ can then be obtained from the slopes of the fitted straight lines, respectively.

From the data with ZnO loading amount of 1.2-8.7% in Table 1, lnk and lnL was plotted and fitted using a straight line in Fig. 11. According to the slope of fitted straight line, α is 0.5193.

According to the data in Table 2, the relationship between lnk and $\ln C_0$ was plotted in Fig. 12. It can be seen from Fig. 12 that a good linear relationship between lnk and $\ln C_0$ is observed with the correlation coefficient higher than 0.99. The slope of fitted straight line reveals that β is −0.3074.

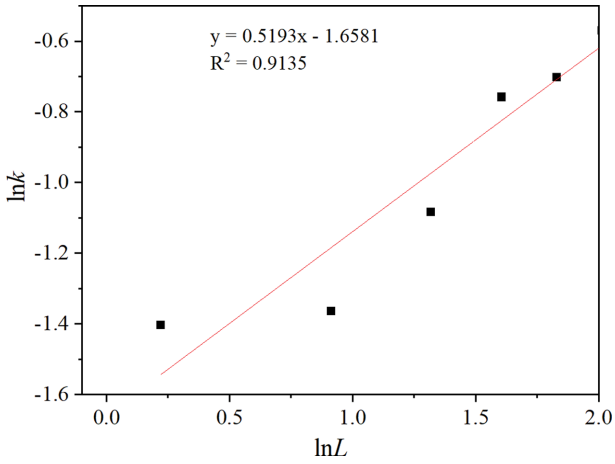

Fig. 11. Relationship between lnk and lnL.

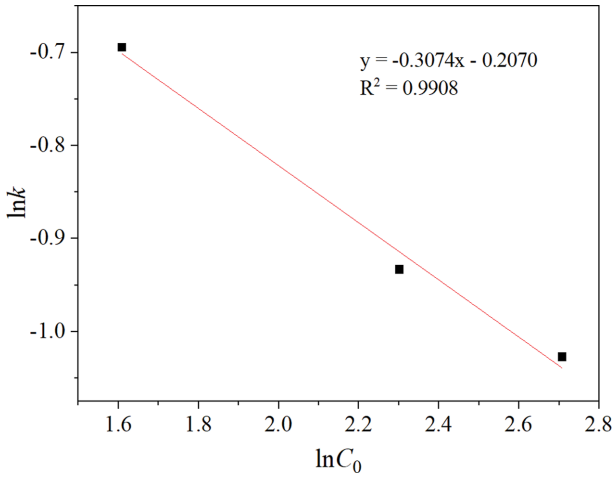

Fig. 12. Relationship between lnk and $\ln C_0$.

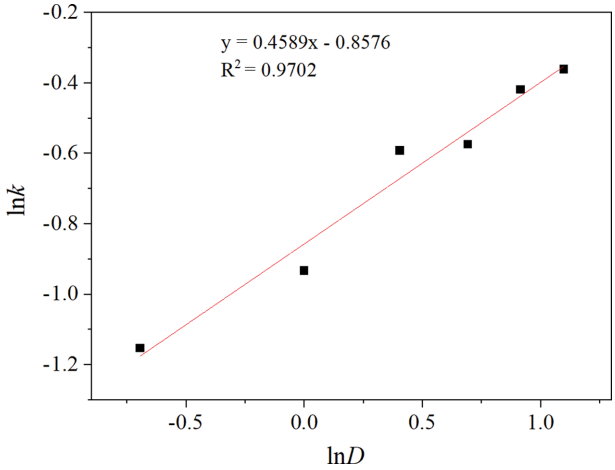

Fig. 13. Relationship between lnk and lnD.

Using the reaction rate k corresponding to different catalyst dosages in Table 3, the relationship between lnk and lnD was plotted and linearly fitted in Fig. 13. It shows that lnk is basically linear

with lnD. It can be obtained from the fitted equation that γ is 0.4589.

The obtained α, β and γ were then introduced into Eq. (5), and Eq. (7) was obtained.

$$k = f(L, C_0, D) = \mu L^{0.5193} C_0^{-0.3074} D^{0.4589} \quad (7)$$

According to Table 1, when the ZnO loading amount L is 8.7%, MB initial concentration C_0 is 10 mg/L (0.01 g/L) and the photocatalyst dosage D is 1 g/L, the reaction rate constant k is 0.6070. When substituting them into Eq. (7), μ was calculated to be 0.5237. As a result, k versus L, C_0 and D was obtained as Eq. (8):

$$k = f(L, C_0, D) = 0.5237 L^{0.5193} C_0^{-0.3074} D^{0.4589} \quad (8)$$

Finally, the reaction kinetic equation of the photocatalytic degradation of MB over ZnO(x)/CSW can be described as follows:

$$\ln C_0/C_t = 0.5237 L^{0.5193} C_0^{-0.3074} D^{0.4589} t \quad (9)$$

CONCLUSION

This work addressed the application of calcium sulfate whisker (CSW) derived from desulfurization gypsum of thermal power plant solid waste to prepare ZnO/CSW photocatalysts for degradation of MB. ZnO/CSW photocatalysts exhibited greatly enhanced photocatalytic activity for degradation of MB than pure ZnO. Among various ZnO(x)/CSW photocatalysts, ZnO(8.7)/CSW had the best photocatalytic activity, over which the MB degradation rate reached 95.4% under optimum conditions. Kinetics study revealed that the photocatalytic degradation of MB over ZnO/CSW followed the pseudo-first-order kinetic model, and the kinetic equation can be described as: $\ln(C_0/C_t)=0.5237L^{0.5193}C_0^{-0.3074}D^{0.4589}t$. Our findings provide a new insight into the recovery of FGD gypsum and offer a possible application of CWS in the photocatalysis field, which is of great significance to environmental protection and high-value utilization of FGD gypsum.

ACKNOWLEDGEMENTS

This work was supported by the National Natural Science Foundation of China (No. 21673290), the Joint Funds of the National Natural Science Foundation of China (No. U1662103) and Beijing Education Committee Science and Technology Project (KM202010017007).

SUPPORTING INFORMATION

Additional information as noted in the text. This information is available via the Internet at http://www.springer.com/chemistry/journal/11814.

REFERENCES

1. S. Wu, W. L. Wang, C. Z. Ren, X. L. Yao, Y. G. Yao, Q. S. Zhang and Z. F. Li, *Constr. Build. Mater.*, **228**, 116676 (2019).
2. M. Miao, X. Feng, G. L. Wang, S. M. Cao, W. Shi and L. Y. Shi, *Particuology*, **19**, 53 (2015).
3. T. T. Fan, X. S. Wang, Y. Gao and X. Y. Zhang, *Constr. Build. Mater.*, **224**, 515 (2019).
4. H. C. Yang, T. P. Tsai and C. T. Hsieh, *Chem. Pap.*, **71**, 1343 (2017).
5. Y. F. Qi, C. F. Zeng, C. Q. Wang, X. B. Ke and L. X. Zhang, *Mater. Lett.*, **194**, 231 (2017).
6. H. Fan, X. F. Song, T. J. Liu, Y. X. Xu and J. G. Yu, *J. Cryst. Growth*, **495**, 29 (2018).
7. Q. J. Zhang, P. Y. Ma, Y. R. Yang, X. F. Pan, J. F. Zhang and L. Xiang, *J. Environ. Chem. Eng.*, **6**, 520 (2018).
8. H. Fan, X. F. Song, Y. X. Xu and J. G. Yu, *Appl. Surf. Sci.*, **478**, 594 (2019).
9. B. L. Cao, X. Wang, X. T. Zhang, B. Jin, Z. Y. Xu, X. P. Liu, W. Zhang and L. S. Yang, *Particuology*, **54**, 173 (2021).
10. G. M. Zeng, M. Chen and Z. T. Zeng, *Science*, **340**, 1403 (2013).
11. M. K. Wang, N. Chamberland, L. Breau, J. E. Moser, R. Humphry-Baker, B. Marsan, S. M. Zakeeruddin and M. Grätzel, *Nat. Chem.*, **2**, 385 (2010).
12. H. Anwer, A. Mahmood, J. Lee, K.-H. Kim, J.-W. Park and A. C. K. Yip, *Nano Res.*, **12**(5), 955 (2019).
13. G. Shilpa, P. K. Mohan, D. K. Kishore, P. R. Deepthi, A. Sukhdev and P. Bhaskar, *Mater. Today: Proc.*, **62**, 5477 (2022).
14. J. Y. Loke, R. S. Mohd Zaki and H. D. Setiabudi, *Mater. Today: Proceed.*, **57**, 1315 (2022).
15. N. M. Julkapli, S. Bagheri and S. B. A. Hamid, *Sci. World J.*, 692307 (2014).
16. C. L. Yu, K. Yang, Q. Shu, J. C. Yu, F. F. Cao and X. Li, *Chinese J. Catal.*, **32**, 555 (2011).
17. M. Khademalrasool, M. D. Talebzadeh and M. Farbod, *J. Photoch. Photobio. A*, **396**, 112561 (2020).
18. Y. S. Liu, W. Gao, C. Zhang, L. Zhang and Y. X. Zhi, *J. Taiwan Inst. Chem. E*, **88**, 277 (2018).
19. M. A. Hernandez-Carrillo, R. Torres-Ricardez, M. F. Garcia-Mendoza, E. Ramirez-Morales, L. Rojas-Blanco, L. L. Diaz-Flores, G. E. Sepulveda-Palacios, F. Paraguay-Delgado and G. Perez-Hernandez, *Catal. Today*, **349**, 191 (2020).
20. L. Song, Y. F. Wang, J. Ma, Q. H. Zhang and Z. J. Shen, *Appl. Surf. Sci.*, **442**, 101 (2018).
21. A. Di Mauro, C. Farrugia, S. Abela, P. Refalo, M. Grech, L. Falqui, V. Privitera and G. Impellizzeri, *Mater. Sci. Semicond. Process.*, **118**, 105214 (2020).
22. W. Zhang, X. Li, H. Wang, Y. J. Song, S. H. Zhang and C. Q. Li, *Korean J. Chem. Eng.*, **34**, 3132 (2017).
23. S. S. Huang, J. R. Zhao, C. H. Wu, X. Wang, S. M. Fei, Q. Zhang, Q. Wang, Z. W. Chen, K. Uvdal and Z. J. Hu, *Chem. Eng. Sci.*, **209**, 115185 (2019).
24. Z. Qin, H. Sun, Y. N. Tang, Z. Y. Chang, S. Y. Yin and Z. N. Liu, *J. Alloys Compd.*, **829**, 154393 (2020).
25. N. Zhang, R. Li, G. Zhang, L. Dong, D. Zhang, G. Wang and T. Li, *Acs Omega*, **5**, 11987 (2020).
26. X. P. Zhang, Q. Q. Wang, J. Li, L. Huang, D. B. Yu and S. J. Dong, *Analyst*, **143**, 2837 (2018).
27. E. Irani and M. Amoli-Diva, *J. Photoch. Photobio. A*, **391**, 112359 (2020).
28. D. Z. Wu, X. M. Fan, J. Dai, H. R. Liu, H. Liu and F. Z. Zhang, *Chinese J. Catal.*, **33**, 802 (2012).
29. H. Niu, D. Zhao, G. Xie, Y. Yuan, W. Zhang, C. Zhang, C. Li and L. Cui, *Fuel*, **304**, 121410 (2021).

30. B. He, X. F. Lin and Y. F. Zhang, *J. Therm. Anal. Calorim.*, **132**, 1145 (2018).
31. Q. J. Guan, W. Sun, R. Q. Liu, Z. G. Yin and C. H. Zhang, *J. Cent. South Univ.*, **25**, 526 (2018).
32. L. P. Ha, T. H. T. Vinh, N. T. B. Thuy, C. M. Thi and P. V. Viet, *J. Environ. Chem. Eng.*, **9**, 105103 (2021).
33. D. Zhou, R. F. Wei, Y. L. Zhu, H. M. Long, B. F. Huang, Y. F. Wang and S. C. Wu, *J. Clean Prod.*, **290**, 125754 (2021).
34. S. M. Patil, S. P. Deshmukh, K. V. More, V. B. Shevale, S. B. Mullani, A. G. Dhodamani and S. D. Delekar, *Mater. Chem. Phys.*, **225**, 247 (2019).
35. X. Li, B. Jie, H. Lin, Z. Deng, J. Qian, Y. Yang and X. Zhang, *J. Environ. Manage.*, **308**, 114664 (2022).
36. S. Dey, S. Das and A. K. Kar, *Mater. Chem. Phys.*, **270**, 124872 (2021).
37. A. Azarniya, M. Soltaninejad, M. Zekavat, F. Bakhshandeh, H. R. M. Hosseini, C. Amutha and S. Ramakrishna, *Mater. Chem. Phys.*, **256**, 123740 (2020).
38. W. Qin, J. Qi and X. H. Wu, *Vacuum*, **107**, 204 (2014).

Supporting Information

Enhanced photocatalytic activity over ZnO supported on calcium sulfate whisker derived from desulfurization gypsum

Shijing Lin*, Yu Tian, Wei Zhang*,†, Tiantian Zhao*, Mingxin Zhao*, and Hong Wang*,†**

*Beijing Key Laboratory of Fuels Cleaning and Advanced Catalytic Emission Reduction Technology, College of New Materials and Chemical Engineering, Beijing Institute of Petrochemical Technology, Beijing 102617, P. R. China
**Beijing Origin Water Membrane Technology Company, Beijing 102617, P. R. China
(*Received 12 February 2022 • Revised 6 June 2022 • Accepted 15 June 2022*)

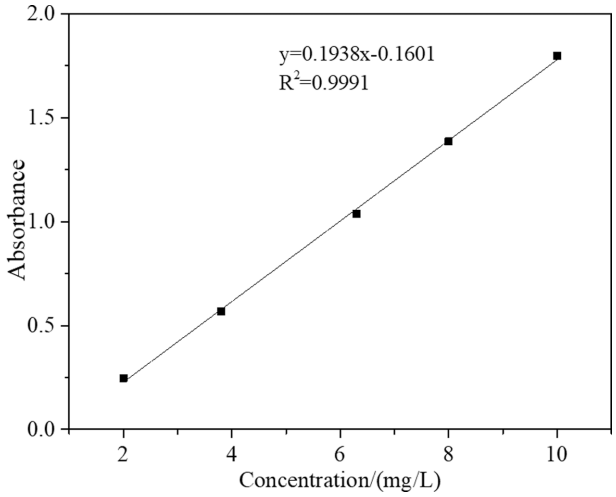

Fig. S1. Standard calibration curve of methylene blue.

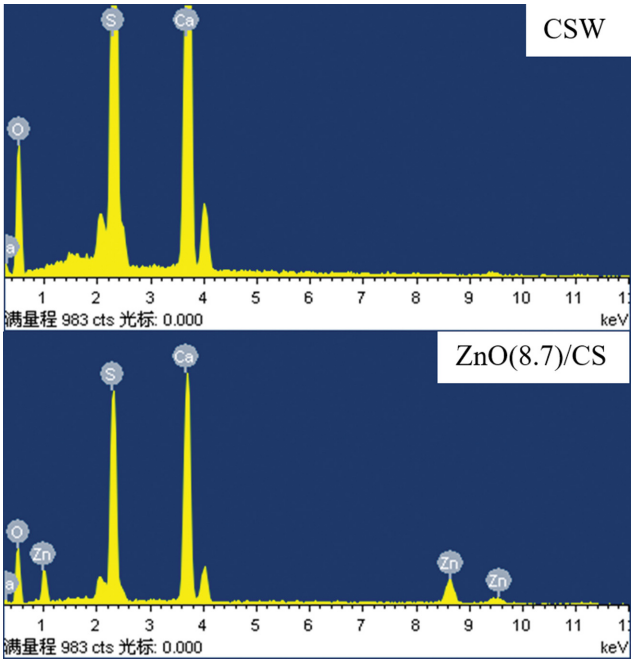

Fig. S2. EDS images of CSW and ZnO(8.7)/CSW.

Table S1. Band gap energies of ZnO(x)/CSW

Sample	E_g/eV	Sample	E_g/eV
CSW	—	ZnO(6.2)/CSW	3.282
ZnO(1.2)/CSW	3.299	ZnO(7.5)/CSW	3.281
ZnO(2.5)/CSW	3.296	ZnO(8.7)/CSW	3.287
ZnO(3.7)/CSW	3.286	ZnO(10)/CSW	3.284
ZnO(5)/CSW	3.283	ZnO(11.2)/CSW	3.272

Table S2. The results of XRD characterization of Zn(x)/CSW

Sample	2θ(°)	FWHM	DXRD (nm)
ZnO(5)/CSW	34.418	0.221	42.2
ZnO(6.2)/CSW	34.402	0.223	38.3
ZnO(7.5)/CSW	34.521	0.246	37.0
ZnO(8.7)/CSW	34.523	0.264	34.0
ZnO(10)/CSW	34.454	0.257	36.2
ZnO(11.2)/CSW	34.483	0.242	37.7

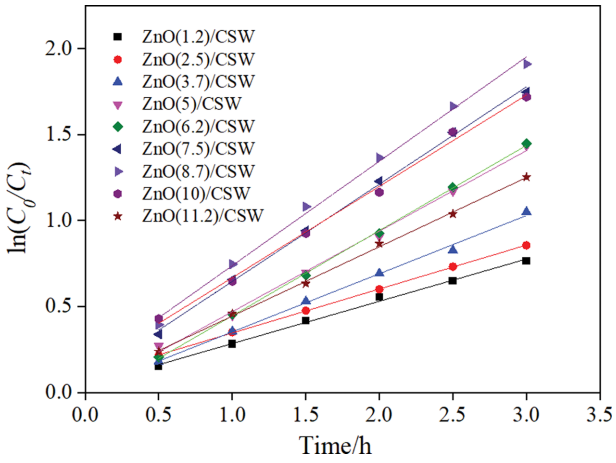

Fig. S3. The pseudo-first-order kinetic fitting of MB photocatalytic degradation over ZnO(x)/CSW with different ZnO loading amounts.

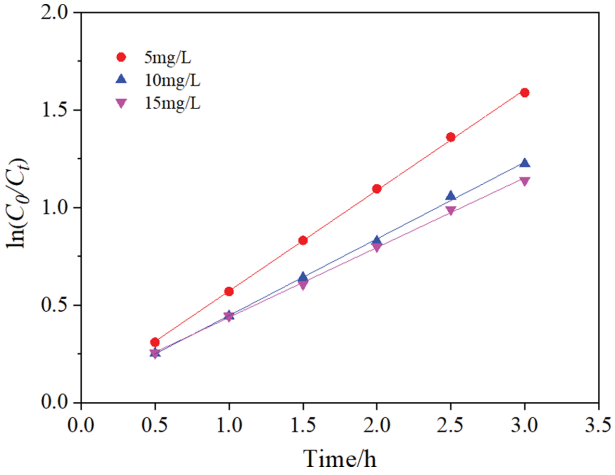

Fig. S4. The pseudo-first-order kinetic fitting of MB photocatalytic degradation with different initial concentrations over ZnO (8.7)/CSW.

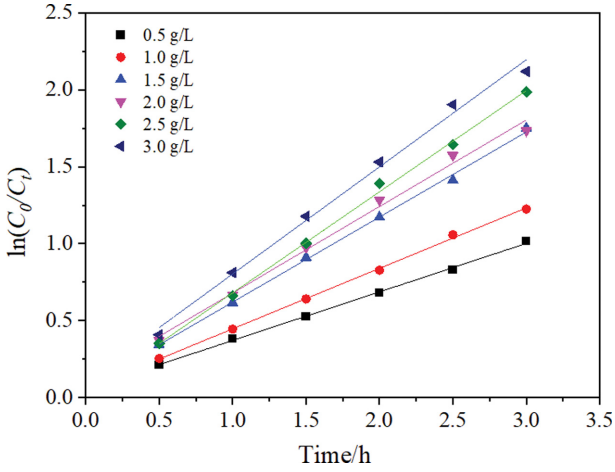

Fig. S5. The pseudo-first-order kinetic fitting of MB photocatalytic degradation under different dosages of ZnO(8.7)/CSW.